Two-dimensional optics : diffraction and dispersion of surface plasmons

Chimento, P.F.

3
Spin-to-orbital angular momentum conversion in a subwavelength slit

We demonstrate partial conversion of circularly polarized light into orbital angular momentum-carrying vortex light with opposite-handed circular polarization. This conversion is accomplished in a novel manner using the birefringent properties of a circular subwavelength slit in a thin metal film. Our technique can be applied over a very wide range of frequencies and even allows the creation of anisotropic vortices when using a slit without circular symmetry.

3.1 Introduction

This chapter was previously published as: Chimento, Alkemade, 't Hooft, and Eliel (2012).

The curious phenomenon of optical vortices arising from axial symmetry in birefringent materials has been studied in uniaxial crystals of variable length,[1] birefringent plates with a spatially varying optical axis and half-wave retardation ("q-plates"),[2] and in annular concentric apertures which resonantly excite surface plasmons.[3] This interaction between spin and orbital angular momentum of light by way of a Berry-Pancharatnam phase has also been studied in space-variant gratings,[4] plasmonic nanostructures in the context of selection rules,[5] and also completely outside the domain of optics, in electron beams.[6]

We present here a novel method of accomplishing this conversion using a subwavelength slit in a metal film acting as a quarter-wave plate, described in chapter 2. We show how this method relaxes the axial symmetry requirement, allowing greater versatility in the form of the vortex created.

In optics, a spin angular momentum of $\pm\hbar$ is associated with a circularly polarized photon. Orbital angular momentum is often associated with an optical vortex beam, where the phase increases azimuthally around the optical axis. These beams have a topological charge Q, equal

[1] Ciattoni et al., 2003; Brasselet, Izdebskaya, et al., 2009.

[2] Marrucci et al., 2006; Karimi, Piccirillo, Marrucci, and Santamato, 2009; Brasselet and Loussert, 2011.

[3] Lombard et al., 2010.

[4] Bomzon et al., 2001.

[5] Gorodetski, Shitrit, Bretner, Kleiner, and Hasman, 2009.

[6] Karimi, Marrucci, et al., 2012.

to the number of full cycles the phase makes in one trip around the optical axis. The expectation value of the orbital angular momentum per photon is $Q\hbar$.[7] The difference between the two forms of angular momentum is beautifully apparent in the interaction of a beam with small particles: interaction with the spin angular momentum in the absence of absorption requires particles that are birefringent; they will start to rotate about their own axis, whereas interaction with a beam carrying orbital angular momentum causes particles, whether birefringent or not, to rotate about the beam's optical axis.[8]

[7] Allen, Beijersbergen, et al., 1992.

[8] O'Neil, MacVicar, Allen, and Padgett, 2002.

CHAPTER 2 DESCRIBES how a subwavelength slit in a metal film can act as an optical retarder. A slit which is subwavelength in one direction, and extended in the other, has two eigenpolarizations: parallel and perpendicular to the slit. By careful design of the slit's width and depth, it is possible to construct a slit that behaves like a quarter-wave retarder for incident light of a certain wavelength, with its fast axis (i.e. axis with the lowest index of refraction) parallel to the orientation of the slit. One can achieve similar results using subwavelength structures with different resonances for orthogonal polarization components.[9] Illuminating the straight slit with circularly polarized light results in linearly polarized light emerging from the other side. The associated change in angular momentum means that a torque is exerted on the sample.[10]

[9] Roberts and Lin, 2012; Genevet et al., 2012.

[10] Beth, 1936.

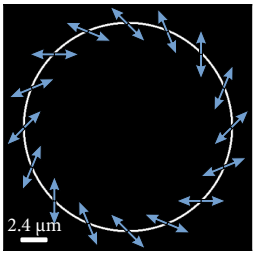

Figure 3.1: Diagram showing the expected local polarization state of light transmitted through the ring slit. The transmitted intensity is constant everywhere on the slit.

When the slit is circular, the fast and slow axes' orientations vary along the slit so that it acts as a space-variant quarter-wave plate. In this circularly symmetric configuration, photonic spin angular momentum cannot transfer to the sample, and must be converted to photonic orbital angular momentum in order to conserve the total angular momentum. This intuitive picture is confirmed by taking the expectation value of the spin and orbital angular momenta per photon,[11] respectively denoted S and L, averaged over the whole beam in the input and output states. Whereas the input state has $S = \hbar, L = 0$, the output state (shown in Fig. 3.1) has $S = 0, L = \hbar$. The total angular momentum per photon, $J = S + L$, is indeed conserved.

[11] Berry, Jeffrey, and Mansuripur, 2005.

3.2 *Near-field experiment*

TO CONFIRM THIS by experiment, we took a glass substrate of 0.5 mm thickness. On it we deposited a titanium adhesion layer of 10 nm thickness, and on that a gold film of 200 nm thickness. We milled a circular slit, 20 µm in diameter and (180 ± 10) nm wide, through the gold film

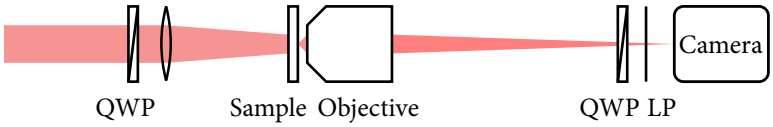

Figure 3.3: Sketch of the experimental setup used to image the ring slit. QWP: quarter wave plate; LP: linear polarizer. The quarter-wave plate and linear polarizer on the right-hand side of the figure measure the local polarization state of the light.

using a focused Ga^+ ion beam. Fig. 3.2 shows a sketch of the structure.

We conducted the experiment using a diode laser with a wavelength of 830 nm. We used a quarter-wave plate to give the beam from this laser a circular polarization state, $\hat{\boldsymbol{\sigma}}_+$. (We define the circular polarization basis unit vectors $\hat{\boldsymbol{\sigma}}_\pm = (\hat{\mathbf{x}} \pm i\hat{\mathbf{y}})/\sqrt{2}$.) We then focused the beam weakly onto the glass side of the sample. The beam diameter at the waist was 90 μm, much larger than the nanostructure diameter of 20 μm, so that, effectively, the structure was illuminated with a plane wave. We used a microscope objective (NA 0.4) to image the slit onto a CCD camera (Apogee Alta U1).

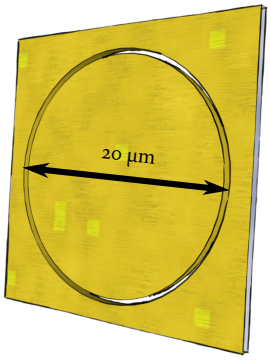

Figure 3.2: A sketch of the nanostructure milled into the sample.

NA: numerical aperture

CCD: charge-coupled device

We measured the polarization of the transmitted light as a function of the transverse position within the image. To determine this polarization, we used a fixed linear polarizer and a computer-controlled rotating quarter-wave plate, as shown in Fig. 3.3, from which we extracted the Stokes parameters according to the method described in Schaefer, Collett, Smyth, Barrett, and Fraher (2007) as a function of position. Fig. 3.4 shows the results of this experiment. We observe small variations in the transmitted intensity along the ring, which are probably caused by small variations in the slit width. The polarization state of the light emerging from the structure, however, shows excellent agreement with the result of our calculations, as shown in Fig. 3.5.

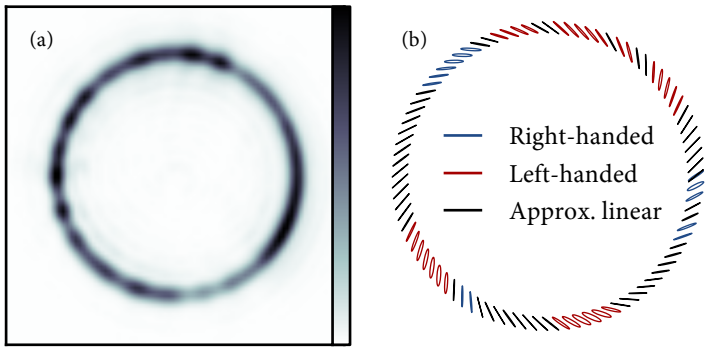

Figure 3.4: (a) Measured intensity transmitted through the ring slit. (b) Local polarization ellipses of the light transmitted through the ring slit. Blue ellipses indicate right-handed elliptical polarization, red ones indicate left-handed elliptical polarization, and black lines indicate polarization states with ellipticity less than 10%.

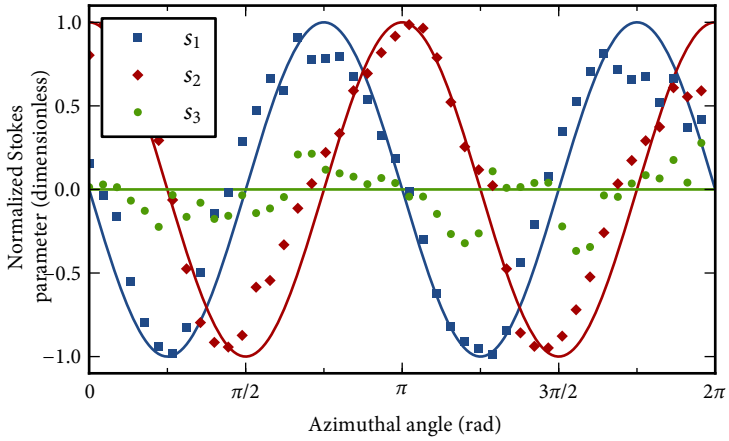

Figure 3.5: Measured normalized Stokes parameters $s_1 = S_1/S_0$, $s_2 = S_2/S_0$, $s_3 = S_3/S_0$ of the light transmitted through the ring slit as a function of azimuthal angle. This shows the same information as Fig. 3.4, but here it is easier to compare it to the expected results (solid lines), with which we observe quite good agreement. An angle of 0° corresponds to 3 o'clock in Fig. 3.4, and increases counterclockwise.

3.3 *Analytical model*

THE POLARIZATION measured in Fig. 3.4 suggests that the light emerging from the nanostructure is a superposition of radial and azimuthal polarization. Beams with such types of polarization, usually called vector beams, were first described as waveguide modes[12] with a dark spot in the center due to a polarization singularity. At first glance, one might expect our metallic nanostructure to produce a vector beam, and thus have a dark spot in the center of the far field. However, calculating the far field by numerical Fourier transform shows that there is no dark spot in the center; in fact, the local polarization state on the optical axis in the far field is purely $\hat{\boldsymbol{\sigma}}_+$, the same as the input polarization state.

[12] Marcatili and Schmeltzer, 1964.

In order to explore this further, we derived an analytical expression for the far field by Fourier-transforming the field shown in Fig. 3.1 and linearizing over the slit width ΔR,

$$\mathbf{E}_0^{\mathrm{FF}} \approx \frac{1+i}{\sqrt{2}} \pi R_0 \Delta R \left(J_0(R_0 k_\perp) \hat{\boldsymbol{\sigma}}_+ - i e^{2i\theta} J_2(R_0 k_\perp) \hat{\boldsymbol{\sigma}}_- \right), \tag{3.1}$$

where R_0 is the radius of the ring, $k_\perp$ the transverse component of the wave vector, and J_n denotes the Bessel function of the first kind of order n. This expression is valid for small ΔR in the paraxial approximation. These fields are visualized in Figs. 3.7(a) and (d). Note that the characteristic length scale in the far field is given by the radius R_0 of the circular structure — that is, the diffraction pattern does not arise from an aperture cutoff, but from the interference between opposite points on the circular slit.

This expression indicates that half of the transmitted beam energy has

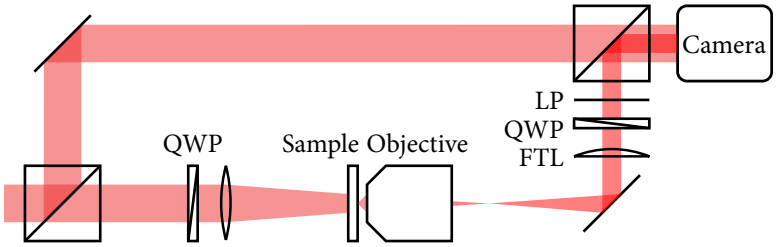

Figure 3.6: Sketch of the experimental setup used to measure the polarization and phase of the far field of the slit. QWP: quarter wave plate; FTL: Fourier-transforming ($2f$) lens; LP: linear polarizer. The objective's focus is now not on the camera but in the focus of the FTL. In this case, the quarter-wave plate and linear polarizer are simply used to view the $\hat{\boldsymbol{\sigma}}_+$ and $\hat{\boldsymbol{\sigma}}_-$ components separately. This configuration also includes a Mach-Zehnder interferometer which measures the phase of each polarization component. When not measuring the phase, we simply block the reference beam.

been converted from the $\hat{\boldsymbol{\sigma}}_+$ to the $\hat{\boldsymbol{\sigma}}_-$ state, while acquiring a topological charge of +2. (The integral of any $J_n(x)$ to infinite x is equal to 1 if $n \geq 0$.) This acquisition of topological charge by the opposite-handed component of the emerging beam can be seen as the result of spin-to-orbital angular momentum conversion, but it is equally instructive to consider it a Berry-Pancharatnam phase, the result of traveling from the north pole ($\hat{\boldsymbol{\sigma}}_+$) of the Poincaré sphere to the south pole ($\hat{\boldsymbol{\sigma}}_-$) through all possible points on the equator, twice.

We confirm this by calculating the expectation values of the spin and orbital angular momenta per photon for both polarization components separately. For the $\hat{\boldsymbol{\sigma}}_+$ component we have $S = \hbar, L = 0$, which is the same as the input state. For the $\hat{\boldsymbol{\sigma}}_-$ component, we have $S = -\hbar, L = 2\hbar$.

3.4 *Far-field experiment*

We performed further experiments to explore this, using a $2f$ system to examine the far field; see Fig. 3.6. We used a quarter-wave plate and a linear polarizer to measure the intensity distribution of the $\hat{\boldsymbol{\sigma}}_+$ and $\hat{\boldsymbol{\sigma}}_-$ components of the far field separately. We also used a misaligned Mach-Zehnder interferometer to visualize the phase of the light transmitted through the slit. The interference pattern consists of parallel interference fringes, which fork according to the topological charge carried by the beam.[13] Figure 3.7 shows the results of our measurements compared to the calculation of (3.1). The interferograms in Figs. 3.7(c) and (f)[14] show that the $\hat{\boldsymbol{\sigma}}_-$ component does indeed have a topological charge of +2, whereas the $\hat{\boldsymbol{\sigma}}_+$ component carries no topological charge.

[13] Basistiy, Soskin, and Vasnetsov, 1995.

[14] In (f), the interference fringe minima are marked in red, using the technique described in Cai, Liu, and Yang (2003).

3.5 *Discussion*

We also consider what happens when the amplitudes of the transmitted polarization components are unequal, or when the retardation is

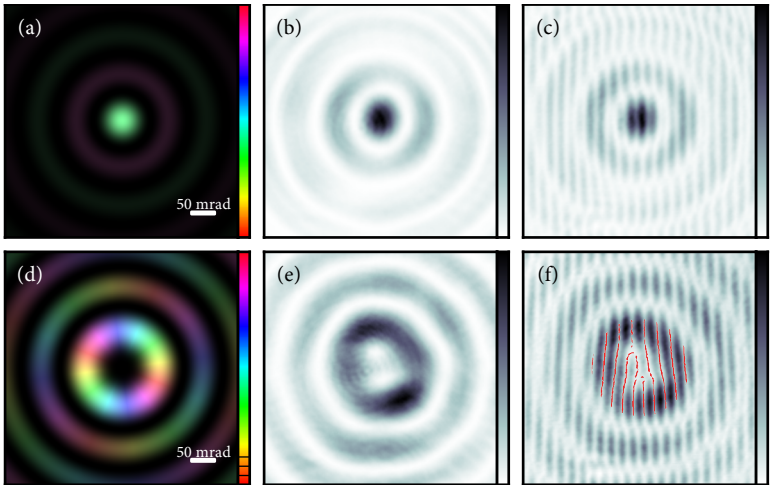

Figure 3.7: Calculated and measured far-field diffraction pattern of the circular slit, split into $\hat{\boldsymbol{\sigma}}_+$ (top row) and $\hat{\boldsymbol{\sigma}}_-$ (bottom row) components. (a, d) Calculated intensity and phase in the far field; luminance indicates intensity, and hue (cycling according to the color bars from 0 through 2π) indicates phase. The $\hat{\boldsymbol{\sigma}}_-$ component has $|Q| = 2$. (b, e): Measured intensity of both components, showing good agreement with the calculations. (c, f): Interferograms using reference beams with appropriate polarization, demonstrating the phase of both components. In (c), the fringes are parallel, indicating a flat wavefront with $Q = 0$. In (f), on the other hand, one fringe splits into three, indicating a helical wavefront with $|Q| = 2$, as in the calculations.

not exactly a quarter wave. We find that the polarization conversion efficiency η is *independent* of the slit's dichroism but depends on the relative phase retardation $\Delta\varphi$ between the polarization components as follows:

$$\eta = I_-/I_{\text{total}} = \sin^2(\Delta\varphi/2), \tag{3.2}$$

where I_- is the intensity of the $\hat{\boldsymbol{\sigma}}_-$ component. If the slit were to behave like a half-wave retarder, then η would become unity. However, designing a half-wave-like slit would once again require careful research to find a suitable width, depth, and material.

This last result suggests that optical spin-orbit conversion is a universal property of a circular nanoslit as long as the local polarization eigenmodes have different propagation constants and are not damped too differently. In order to obtain 100% conversion efficiency one obviously has to adjust the properties of the slit to the wavelength of the incident light in a way similar to the design of a liquid-crystal based q-plate[15] for a certain wavelength. An attractive benefit of this approach to optical spin-orbit conversion is that it is universal, i.e. it can be used at wavelengths from the deep UV to the far infrared.

[15] Marrucci et al., 2006.

One may wonder what happens when the metallic nanoslit is no longer cylindrically symmetric but encircles a singly connected domain. Since the circular symmetry is broken, transfer of angular momentum to the sample is no longer forbidden. For a quarter-wave-like slit with a circularly polarized Gaussian beam incident on it, half of the emerging light will have the opposite circular polarization and carry a charge 2 vortex

with a broad orbital angular momentum spectrum. Contrary to the case of a circular slit, this vortex will be anisotropic.

3.6 Summary

We have demonstrated spin-to-orbital angular momentum conversion of an electromagnetic field upon transmission through a circular metallic nanoslit. When illuminated with circularly polarized light, part of the field transmitted through the slit is converted to the opposite handedness and its topological charge is increased or decreased by 2, corresponding to a conversion of spin angular momentum to orbital angular momentum. The conversion efficiency is a function of the relative phase delay that the slit imposes on orthogonal polarization components. This means that full spin-orbit conversion could be achieved simply by passing the light through a slit in a thin metal film, if the slit were to behave like a half-wave retarder. Using a slit without circular symmetry, on the other hand, opens up a new world of possibilities for creating anisotropic optical vortices.

Appendix 3.A Plasmon-assisted transmission

This section is an appendix that did not appear in the published paper.

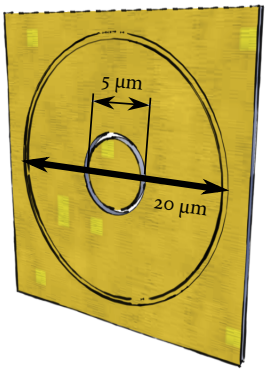

Figure 3.8: A sketch of the groove-slit nanostructure milled into the sample.

We also conducted experiments on a ring slit similar to the one in Fig. 3.2, with an added groove which serves as a surface plasmon outcoupler. On the same substrate, we milled a circular slit, 5 μm in diameter and 200 nm wide, and then a circular groove concentric with the slit, 20 μm in diameter and also 200 nm wide. The groove is essentially a slit which is not deep enough to reach all the way through the gold layer. Due to the focused-ion beam being depth-calibrated for silicon substrates and not gold, the exact depth of the groove is uncertain, but we estimate (100 ± 25) nm. Fig. 3.8 shows a sketch of this structure.

Since the slit's quarter-wave plate-like behavior relies strongly on the loss due to surface plasmon generation, we can expect surface plasmons to travel radially outwards from the slit. When these surface plasmons reach the groove, they are partly scattered into free space as propagating light. We expect this light to be radially polarized around the symmetry axis of the slit. To measure this scattering, we conducted the experiment in exactly the same way as described in section 3.2, except that we overexposed the CCD camera in order to detect the much weaker scattering from the groove.

Figures 3.9 and 3.10 show the results of this experiment. The transmitted intensity (Fig. 3.9a) is more complicated to interpret in this case. For one thing, it exhibits blooming[16], which blots out a small section of the groove.

[16] Blooming is the vertical streaking visible when overexposure causes too many electrons to accumulate in the potential well of a CCD pixel, making them overflow to neighboring pixels.

Also, the slit and groove are subwavelength, making it impossible to image them perfectly. In practice, this means that the crisp boundaries of the slit and groove are softened and widened, and unwanted garbage shows up on the camera outside of the slit and groove. The usual way

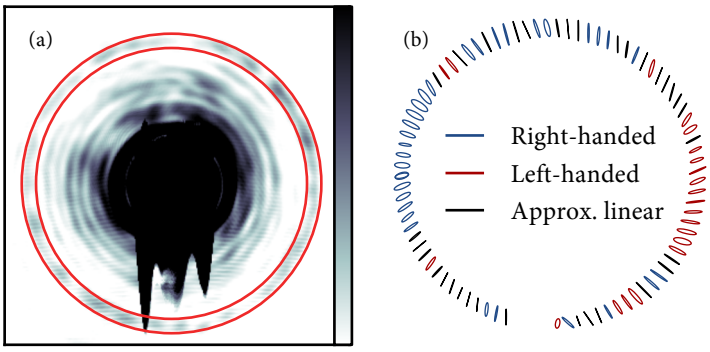

Figure 3.9: (a) Measured intensity emitted by the ring groove (delineated in red). The light transmitted through the smaller ring slit is obscured by blooming due to overexposure. (b) Local polarization ellipses of the light emitted by the ring groove. Blue ellipses indicate right-handed elliptical polarization, red ones indicate left-handed elliptical polarization, and black lines indicate polarization states with ellipticity less than 10%.

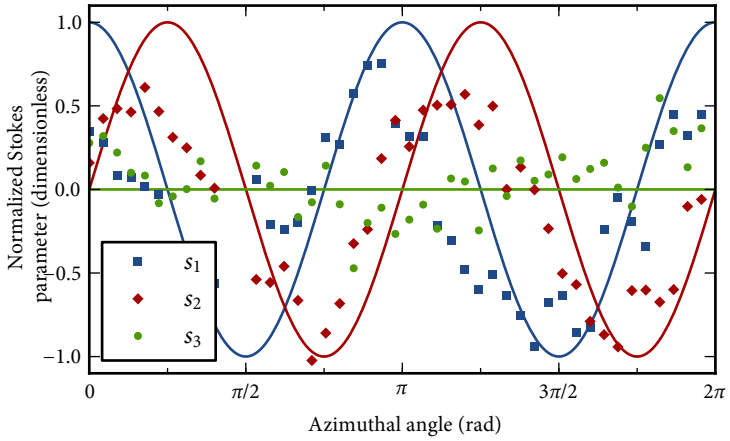

Figure 3.10: Measured normalized Stokes parameters $s_1 = S_1/S_0$, $s_2 = S_2/S_0$, $s_3 = S_3/S_0$ of the light emitted by the ring groove as a function of azimuthal angle. This shows the same information as Fig. 3.9, but here it is easier to compare it to the expected results (solid lines). Compare Fig. 3.5.

of explaining this phenomenon is to define a PSF for the imaging system. The PSF can also be viewed as the impulse response of the imaging system, the impulse being an infinitesimal point source. The source field can then be viewed as a superposition of infinitesimal point sources, and the field at the image plane of the imaging system is a superposition of point spread functions. In other words, the output field is the convolution of the input field with the point spread function. The intensity point spread function of an ideal imaging system is an Airy disc.[17] In Fig. 3.4a, the point spread function is barely visible, because the outer rings of the Airy function are very faint, but since the light emerging from the groove is much fainter than the slit, they are of comparable intensity. Therefore, the groove is marked in Fig. 3.9a in between two concentric circles.

PSF: point-spread function

Taking into account that the polarization measurements in Fig. 3.9 are less accurate than those in Fig. 3.4, we still note that the groove emits light that is more or less radially polarized. We compare the measurements to the expectation in Fig. 3.10.

Here, also, we calculate the expectation value of the spin and orbital angular momenta per photon averaged over the whole beam in the output state of the plasmon-assisted transmitted light, shown in Fig. 3.10. This output state has $S = 0, L = \hbar$, again showing that the total angular momentum per photon, $J = S + L$, is conserved.

[17] When dealing with the field, one should actually use a complex 3-vector-valued point spread function (Marian et al., 2007), but here we will assume that there is no coupling between TE and TM components due to the imaging system.

Appendix 3.B Plasmonic cross-talk between points on the ring

This section is an appendix that did not appear in the published paper.

CONSIDERING THE PLASMONIC CONTRIBUTION in the slit-only system may also help to explain why the polarization in Fig. 3.4b is not purely

linear. The light incident on the slit is converted linearly to a surface plasmon, barring an unknown attenuation and retardation factor which we will ignore for now. These surface plasmons travel from one side of the circle to the other.

TM: transverse magnetic

Only the TM component excites a plasmon, with $\hat{\mathbf{z}}$-polarization. The plasmon propagates across the gold surface, undergoing diffraction, and hits the slit again, scattering once again into TM, or $\hat{\mathbf{r}}$-polarized, light. Since the plasmons only couple to radial polarization, the plasmonic contribution to the transmission has a different polarization than the direct contribution. The smaller plasmonic contribution should therefore be visible as a deviation in the polarization of the light emerging from the slit.

To calculate the diffraction the surface plasmons undergo during the transit from one side of the ring to the other, we look at the Fresnel-Kirchhoff diffraction integral: [18]

[18] As in Griffiths (1999), $\boldsymbol{\imath}$ denotes the separation vector between a source point $\mathbf{r}'$ and a field point $\mathbf{r}$: $\boldsymbol{\imath} \equiv \mathbf{r} - \mathbf{r}' = (x-x')\hat{\mathbf{x}} + (z-z')\hat{\mathbf{z}}$.

$$E(x,z) = \frac{1}{i\sqrt{\lambda_{SP}}} \int E(x',0) \frac{e^{ik\boldsymbol{\imath}}}{\sqrt{\boldsymbol{\imath}}} \cos\eta \, dx'$$

Since the diffraction takes place in two dimensions, the Huygens waves scattered by each point on the wavefront are not spherical (e^{ikr}/r) but instead damped cylindrical waves[19] ($e^{ikr}/\sqrt{r}$). Here, z is the diffraction distance along the propagation axis. The separation vector $\boldsymbol{\imath}$ is the distance between a source point x' in the $z = 0$ plane and the point x that we are interested in in the image plane. The angle $\eta = \arccos z/\boldsymbol{\imath}$ is the angle between the propagation vector and the separation vector, so $\cos\eta$ can also be written as $\hat{\mathbf{k}} \cdot \hat{\boldsymbol{\imath}}$.

[19] Teperik, Archambault, Marquier, and Greffet, 2009.

Based on this, we can construct the following diffraction integral in polar coordinates for our ring-slit geometry, shown in Fig. 3.11:

$$E_{SP}(R_0,\theta) = \frac{1}{i\sqrt{\lambda_{SP}}} \int_{-\pi/2}^{\pi/2} E_{0,SP}(R_0, \theta+\zeta) \frac{e^{ik_{SP}\boldsymbol{\imath}}}{\sqrt{\boldsymbol{\imath}}} \hat{\mathbf{k}} \cdot \hat{\boldsymbol{\imath}} R_0 \, d\zeta \tag{3.3}$$

The physical meaning of this integral is that for each point on the ring, the surface plasmon-assisted field is a sum of the contributions from points elsewhere on the ring. The point (R_0, θ) that we are interested in only receives contributions from the facing inner side of the ring: angles $\theta+\pi/2$ to $\theta + 3\pi/2$.

After some calculation, we can write:

$$E_{SP}(R_0,\theta) = iE_{0,SP}(R_0,0)\tilde{f}(k_{SP}R_0) \tag{3.4}$$

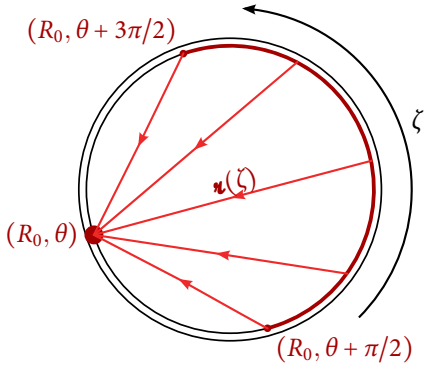

Figure 3.11: Diffraction geometry of surface plasmons traveling inside the circular slit from one side to the other. The plasmon-assisted transmission at each point on the ring (R_0, θ) is the sum of contributions from the plasmonic field launched on the semicircle opposite on the ring. When converted back to light, this plasmonic contribution should be purely radially polarized, which should be visible as an alteration of the polarization direction of the directly transmitted contribution.

where

$$\tilde{f}(q) = \frac{1}{4}\sqrt{\frac{q}{\pi}} \int_{-\pi/2}^{\pi/2} e^{i(\zeta + 2q\cos(\zeta/2))} \frac{1+\cos\zeta}{(\cos(\zeta/2))^{3/2}}\, d\zeta$$

Adding the direct and plasmonic contributions, we see that the light emerging from the slit is not necessarily linearly polarized anymore:

$$\tilde{\mathbf{E}}_{0,\text{out}}(R_0, \theta) = \frac{i}{\sqrt{2}} e^{i\theta} \left(\left(1 + \tilde{A}\tilde{f}(k_{\text{SP}} R_0)\right) \hat{\mathbf{r}} + \hat{\boldsymbol{\theta}} \right) \tag{3.5}$$

where $\tilde{A}$ is the unknown attenuation and retardation due to conversion between light and surface plasmons and vice versa. The plasmonic contribution adds a small degree of ellipticity to the polarization everywhere, depending on the phase of $\tilde{A}$.